Interaction of Neutrons with He^3†

A. R. SAYRES, K. W. JONES,* AND C. S. WU
Columbia University, New York, New York

(Received February 7, 1961)

Spectra of the $n+He^3$ reactions were obtained for monoenergetic neutron fluxes of 0.95, 2.67, 5.00, 8.07, and 17.5 Mev using a He^3-filled proportional counter. Analysis of these spectra yielded the ratios to the total cross section of the total elastic, the $He^3(n,p)H^3$, and the $He^3(n,d)D$ reaction cross sections. Absolute cross sections were obtained by normalization to the known total cross section. Differential elastic-scattering cross sections for neutrons on He^3 were obtained through the relationship between the scattering angle of the neutron and the observed energy of the He^3 recoil in the counter filling. These angular distributions are compared with the theoretical angular distributions as calculated by Bransden, Robertson, and Swan. The present experiment was intended to discriminate between their assumed two special cases for the potential interaction, the symmetrical exchange force and the Serber exchange force. The experimental results favor the Serber exchange force. This experiment also was intended to make possible the analysis of more complex neutron spectra by providing knowledge of $n+He^3$ reaction cross sections and the spectra obtained when only monoenergetic neutrons are present. A comparison is made of the results of this experiment with cross sections calculated from inverse reactions and direct measurements of other investigators, where such data are available.

I. INTRODUCTION

A CONSIDERABLE amount of theoretical and experimental data is now available concerning the elastic scattering of nucleons by deuterons and alpha particles.[1] The experimental data are shown to be inconsistent with the assumption of mainly ordinary forces. However, from the data, it is difficult to decide what exchange potential best describes the nuclear interaction.

Bransden, Robertson, and Swan have calculated angular distributions for the elastic scattering of neutrons by He^3 and H^3.[2] They applied the method of "resonating group structure"[3] to build up a wave function for the nuclei, and assumed a purely central potential consistent with the binding energies of the deuteron and alpha particle. The possible $p+H^3$ and $D+D$ groupings were not included in the wave function.

The two special cases for the potential interaction investigated by Bransden *et al.* are the symmetrical exchange force and the Serber exchange force. The phase shifts and the corresponding angular distributions for the elastic scattering of neutrons by He^3 have been calculated for incident neutron energies of 1.0, 2.5, 5.0, 8.0, and 14.0 Mev. For the two types of exchange forces used, quite different angular distributions and total elastic-scattering cross sections were obtained. One would therefore expect that experimental data for the scattering of neutrons by He^3 should make a distinction between the symmetrical and Serber type exchange forces. While experimental data for the elastic scattering of neutrons by H^3 have been available at 14 Mev,[4] the measurements were in the angular interval between 67° and 180° where the differential cross sections at this energy appear insensitive to the type of force.

The present experiment was undertaken primarily to furnish data which would provide a more sensitive test of the theoretical cross sections over a wide range of neutron energies. Knowledge of these cross sections and a series of spectral distributions due to monoenergetic neutrons of various energies will facilitate the interpretation of the results obtained from using the n-He^3 reaction for a neutron spectrometer[5] and extend the neutron energy region to which this technique may be applied. In such a spectrometer, at energies above 1 Mev and especially above 4.4 Mev, care must be exercised to identify the $He^3(n,p)H^3$ and $He^3(n,d)D$ reaction peaks and the maximum of the recoil distribution for each energy group of the incident neutrons. With knowledge of the spectra obtained for a single-neutron energy, a He^3-filled proportional counter may then be used above 1 Mev as a neutron spectrometer in cases where a few neutron groups are present.

A He^3-filled proportional counter gives a convenient method of determining the cross sections for the $He^3(n,p)T$, $He^3(n,d)D$, and the $He^3(n,n)He^3$ processes. In the first two cases, if the charged particle reaction products are stopped within the sensitive volume of the counter, a single energy peak is produced whose pulse height is proportional to the neutron energy plus the Q of the reaction. For the elastic scattering, the recoil He^3 nuclei will give a distribution in energy which ranges from zero to $\frac{3}{4}E_n$. From the kinematics of the process, one finds that a measurement of the recoil-energy distribution is equivalent to a measurement of the angular distribution for elastic scattering in the center-of-mass system. In general, the use of the

† This work partially supported by the U. S. Atomic Energy Commission.

* Now at The Ohio State University, Columbus, Ohio.

[1] A. H. de Borde and H. S. W. Massey, Proc. Phys. Soc. (London) **A68**, 769 (1955). K. B. Mather and P. Swan, *Nuclear Scattering* (Cambridge University Press, New York, 1958).

[2] B. H. Bransden, H. H. Robertson, and P. Swan, Proc. Phys. Soc. (London) **A69**, 877 (1956).

[3] J. A. Wheeler, Phys. Rev. **52**, 1083 (1937); H. M. Parker, M.A. thesis, University of North Carolina, 1937 (unpublished). J. A. Wheeler, Phys. Rev. **52**, 1107 (1937).

[4] J. H. Coon, C. K. Bockelman, and H. H. Barschall, Phys. Rev. **81**, 33 (1951).

[5] R. Batchelor, R. Aves, and T. H. R. Skyrme, Rev. Sci. Instr. **26**, 1037 (1955).

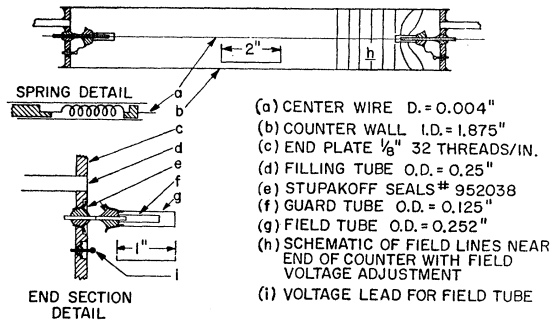

FIG. 1. Proportional counter and details of construction.

proportional counter requires a relatively small amount of He^3 and gives reaction cross sections which could not be obtained if a separate scatterer-detector system were used. This type of experiment yields only relative cross sections. To obtain absolute cross sections, the total neutron cross section must be known. The total cross section data were available at all neutron energies used in this experiment.[6]

In the present experiment, differential cross sections for the elastic scattering of neutrons by He^3 were obtained at 2.6, 5.0, 8.0, and 17.5 Mev. The $He^3(n,p)H^3$ cross section was measured at 1.0, 2.6, 5.0, and 8.0 Mev, and the $He^3(n,d)D$ cross section (threshold at $E_n=4.36$ Mev) was measured at 5.0 and 8.0 Mev. A comparison of the measured cross sections with theory and other experimental data is presented.

II. EXPERIMENTAL PROCEDURE

A. Observation of $n+He^3$ Reactions

A proportional counter (see Fig. 1) with a partial filling of He^3 was bombarded by neutrons produced by the $T(p,n)He^3$, $D(d,n)He^3$, and $T(d,n)He^4$ reactions. Spectra of the $n+He^3$ reactions were recorded on a 256-channel analyzer. The neutron energies, the reactions used to obtain the neutrons, and the energy losses of the Van de Graaff beam in the gas targets and entrance foils are listed in Table I.

The gas fillings used in the proportional counter are listed in Table II. The krypton was used to stop the $n+He^3$ reaction products. After purification, the gas was found to be better than 99.99% pure with less than one part in 10^{11} tritium contamination left in the He^3. Details of the construction and operation of the proportional counter and the gas filling system and gas purification are described elsewhere.[7]

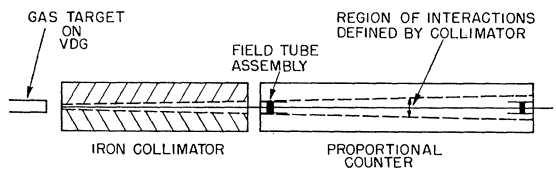

FIG. 2. Schematic diagram of the experimental arrangement of the neutron source, neutron collimator, and neutron detector.

[6] L. Cranberg *et al.*, Los Alamos Scientific Laboratory Report LA-1853, 1954 (unpublished).

TABLE I. Neutron sources and the beam-energy loss in the targets.

Neutron energy in lab system E_n (0°); (Mev)	Reaction	Half-thickness of gas target for bombarding particle (kev)	Thickness of entrance foils for bombarding particle (kev)
0.95±0.02	$H^3(p,n)He^3$	19	193
2.67±0.02	$H^3(p,n)He^3$	11	126
5.00±0.02	$H^3(p,n)He^3$	7	92
8.07±0.02	$D(D,n)He^3$	14	80
17.50±0.05	$H^3(D,n)He^4$	33	276

Collimators were used, as illustrated schematically in Fig. 2, to confine the neutron flux to the region along the axis of the proportional counter. This reduced the counter "wall effect," i.e., reduced the number of $n+He^3$ events whose final reaction products hit the walls of the proportional counter and consequently expended only part of their kinetic energy in the gas volume. The materials and dimensions of these collimators are listed in Table III.

Backgrounds due to neutrons scattered into the detector from the collimator or from the room were observed by replacing the collimator with a solid cylinder of the same material and outside dimensions.

The general features of the spectrum obtained from the proportional counter are illustrated for incident neutrons of energy 2.5 Mev in Fig. 3. A peak due to the $He^3(n,p)H^3$ reaction occurs at a pulse height corresponding to an energy E_n+Q. The full width at half maximum is 5% of the pulse height, giving 7.3% resolution for neutrons of 2.5-Mev energy. The maximum of the recoil He^3 distribution occurs at $E_R=\frac{3}{4}E_n$. Backgrounds due to epithermal neutrons which give a peak at the energy corresponding to the Q of the $He^3(n,p)H^3$ reaction, and the interactions of neutrons and gamma rays with krypton and CO_2 are also shown.

B. Recording of the Data

For each energy, spectra were obtained with a lead or iron collimator and then with a solid cylinder of the same material and over-all dimensions. Identical pairs of runs were then taken with all but a small amount of He^3 removed from the counter filling in order to determine the backgrounds due to Kr and CO_2 recoils and

TABLE II. Gas fillings.

E_n (Mev)	He^3 (in. Hg)	Kr (atm)	CO_2 (in. Hg)
2.6, 5.0, 17.5	29.0	4.0	1.25
2.6, 5.0, 17.5	0.4	4.25	1.33
8.0	29.7	4.0	1.25
8.0	1.5	4.25	1.33

[7] A. R. Sayres, thesis, Atomic Energy Commission Report CU(PNPL)-200, 1960 (unpublished).

TABLE III. Collimators.

Collimator	Material	Length (in.)	Diameter of Cylinder (in.)	Entrance aperture (in.)	Exit aperture (in.)
A	Iron	7.9	2.0	0.14	0.28
B	Lead	7.9	2.0	0.15	0.31
C	Lead	7.9	2.0	0.26	0.48
D	Boron and paraffin	9.0	2.0	0.5	0.5

the interactions of gamma rays with the counter gases. The small amount of He^3 present was enough to give a point of energy calibration from the $He^3(n,p)H^3$ reaction with the epithermal neutrons, which passed through a cadmium foil surrounding the proportional counter.

In order to illustrate the recording of the data, a set of runs for $E_n=8.0$ Mev will be discussed, since at this energy all details of the experiment are present. Then features characteristic of a specific incident-neutron energy will be pointed out.

An iron collimator (see Table III, collimator *A*) was placed between the deuterium gas target neutron source and the proportional counter, as illustrated in Fig. 2. The gas filling was 1 atm He^3, 4 atm Kr, 1.25 in. Hg of CO_2. The spectrum for an integrated beam charge of 2200 μcoul is shown in Fig. 4, curve (a); the spectrum obtained when the collimator was replaced by a solid cylinder is shown by curve (b). All runs were monitored with a "long counter," placed at 90° with respect to the beam direction, so that backgrounds to be subtracted could be properly normalized.

Contamination of the neutron flux arising from the interaction of the Van de Graaff beam with target assembly materials other than the gas filling was examined using the He^3-filled proportional counter and found to be negligible, except in the case of the $D(d,n)He^3$ reaction used to obtain E_n(lab)=8.0-Mev neutrons. In this case, the deuterium in the gas target was replaced by He^4, and a similar set of data was taken. The small background to be subtracted is the difference between curves (a), data taken with the iron collimator, and (b), data taken with the solid iron cylinder, as shown in Fig. 5. The differences between

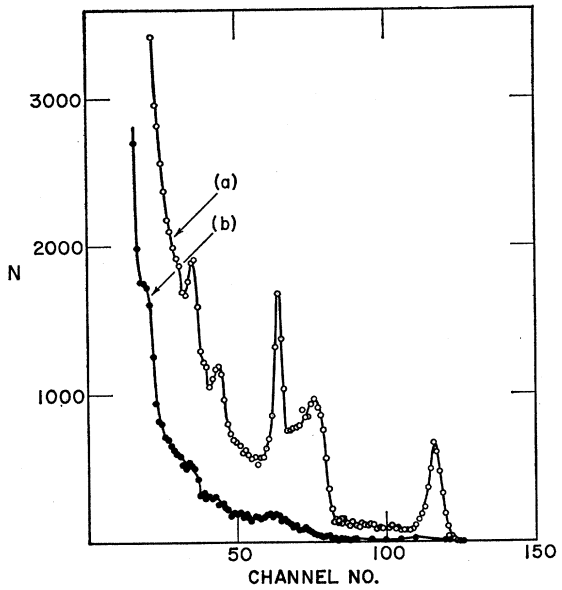

FIG. 4. The spectrum obtained for $E_n=8.0$ Mev with the neutron spectrometer, using the collimator *A* [curve (a)] and using the solid iron cylinder [curve (b)].

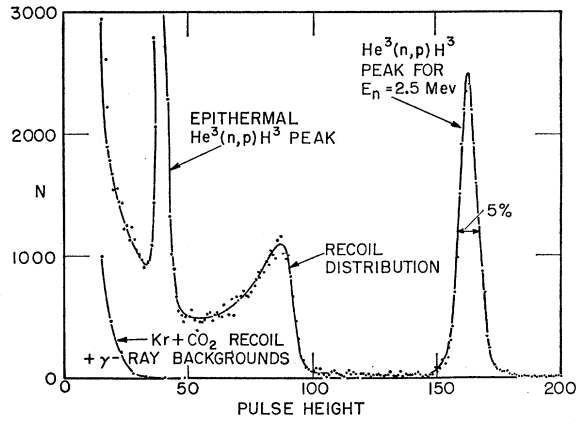

FIG. 3. Neutron spectrum observed with the He^3-filled proportional counter using 2.5-Mev neutrons from the $H^3(p,n)He^3$ reaction. Backgrounds in the absence of He^3 are also shown. The curves shown are the differences between runs taken with a collimator and a solid cylinder.

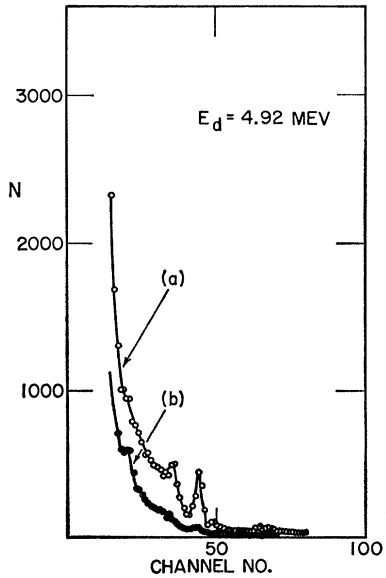

FIG. 5. The neutron background, for data at $E_n=8.0$ Mev, produced in the gas target materials by 4.92-Mev deuterons as observed by the spectrometer, using collimator *A* [curve (a)] and using a solid iron cylinder [curve (b)].

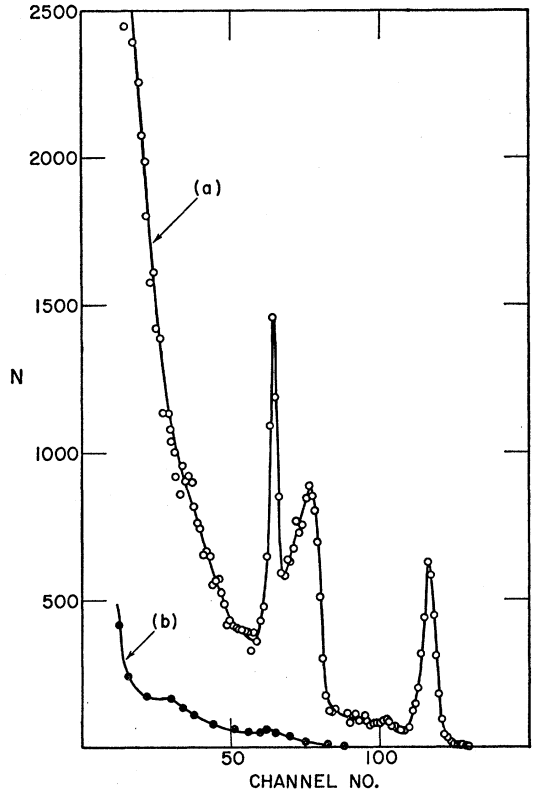

FIG. 6. For $E_n=8.0$ Mev, curve (a) shows the spectrum of neutron and gamma-ray interactions with the gas filling of the spectrometer, i.e., the following combination of the data: Figs. (4a–4b)–(5a–5b). Curve (b) shows the spectrum of neutron and gamma-ray interactions obtained from a similar set of curves in the absence of He^3 in the spectrometer.

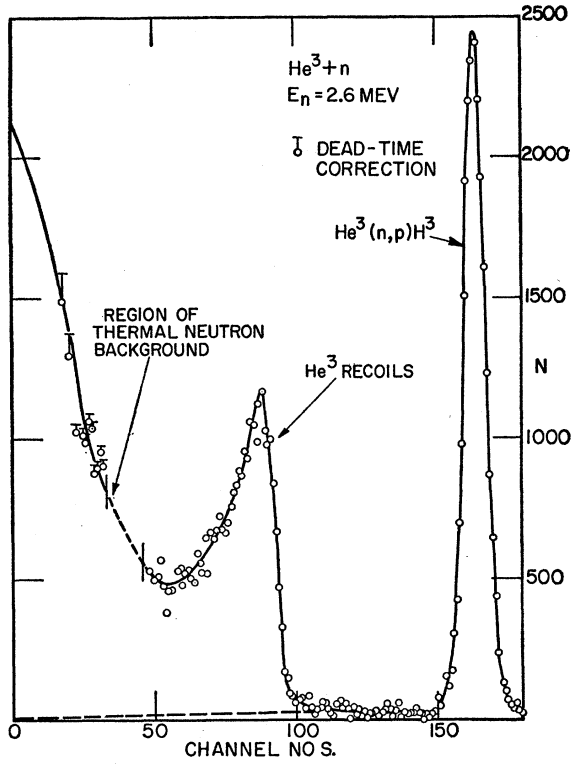

FIG. 7. The spectrum of the interaction of 2.67-Mev neutrons with He^3. The dead-time corrections for the counting rates used are shown. The calculated wall-effect spectrum for the $He^3(n,p)H^3$ reaction is shown as a dashed curve.

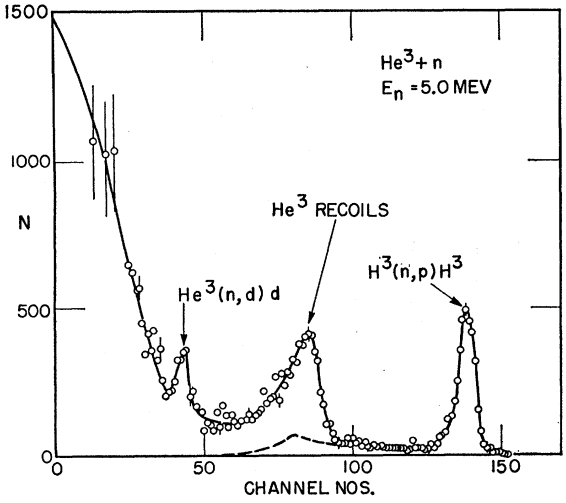

FIG. 8. The spectrum of the interaction of 5.00-Mev neutrons with He^3. The calculated wall-effect distribution for the $He^3(n,p)H^3$ reaction is shown as the dashed curve.

curves (a) and (b) of Figs. 4 and 5 were then subtracted from each other. The result is shown as curve (a) of Fig. 6.

With a gas filling 1.5 in. Hg of He^3, 4.25 atm Kr, and 1.33 in. Hg of CO_2, the procedure was repeated. This provided the spectrum of the interaction of the neutrons with the krypton and CO_2, and also gamma rays with the counter gas. The result is shown as curve (b) in Fig. 6. The difference between curves (a) and (b) of Fig. 6 is plotted in Fig. 9, which shows the final spectrum of events obtained for the interaction of 8.0-Mev neutrons with He^3.

The over-all procedure was performed twice to provide a check of stability of the apparatus. The data were found to be reproducible. The energy region corresponding to the thermal-neutron background has been omitted, because this large background masks the recoil distribution. A smooth curve is drawn through the data and extrapolated to zero energy. The effect of this extrapolation on the final results is discussed below.

A spectrum for $E_n=1.0$ Mev was obtained using $T(p,n)He^3$ neutrons. The $He^3(n,p)H^3$ cross section at this energy was obtained by using the "long counter" to normalize the yield at 1 Mev to that obtained for the $He^3(n,p)H^3$ reaction at 2.6 and 5.0 Mev. The elastic-scattering cross section for $E_n=1.0$ Mev was then obtained by subtracting σ_{np} from σ_{total}.

Corrections for the effect of the dead time of the pulse-height analyzer were found to be negligible for

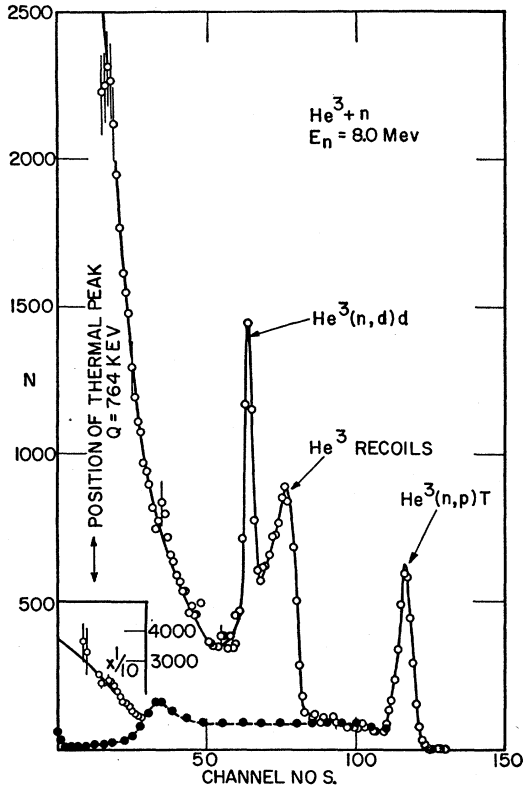

FIG. 9. The spectrum of the interaction of 8.07-Mev neutrons with He^3 [curve (a) minus curve (b) of Fig. 6]. The calculated wall-effect distribution for the $He^3(n,p)H^3$ reaction is shown as the dashed curve.

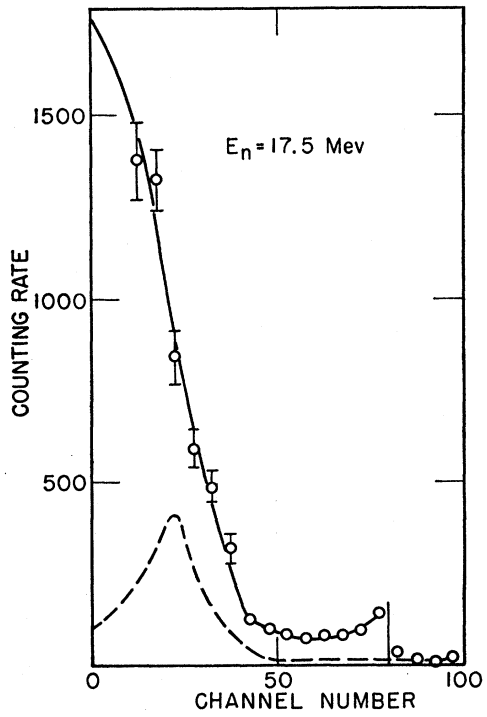

FIG. 10. The spectrum of the interaction of 17.50-Mev neutrons with He^3. The calculated wall-effect distribution for the $He^3(n,p)H^3$ and $He^3(n,d)D$ reactions is shown as the dashed curve.

the counting rates used at all neutron energies except at $E_n=2.6$ Mev. The magnitude of the correction, in this case, is indicated in Fig. 7, in which is plotted the spectrum of events obtained for the interaction of 2.6-Mev neutrons with He^3. This spectrum was obtained in a manner similar to that used for $E_n=8.0$ Mev.

The spectra of $n+He^3$ events at $E_n=5.0$, 8.0, and 17.5 Mev, similarly obtained, are shown in Figs. 8, 9, and 10, respectively. At $E_n=5.0$ Mev, a peak appears corresponding to the $He^3(n,d)D$ reaction whose threshold is at $E_n=4.36$ Mev. (See Fig. 8.) At $E_n=8.0$ Mev, this reaction peak appears sharply resolved in the midst of the He^3-recoil distribution. (See Fig. 9.) At $E_n=17.5$ Mev, the wall effect for both the $He^3(n,p)H^3$ and $He^3(n,d)D$ reactions was so large that no peaks were observed. (See Fig. 10.)

C. Correction of the Spectra for Distortion Due to Wall Effect

In order to separate those portions of the observed spectra that correspond to elastic and inelastic events, and to determine the wall-effect corrections to be applied to the shape of the He^3 recoil pulse-height distributions, it was necessary to calculate the distribution expected for monoenergetic incident-neutron fluxes as modified by particles of the $n+He^3$ reactions hitting the walls of the proportional counter. The expected spectrum was calculated for each of the following reactions: $He^3(n,n)He^3$, $He^3(n,p)H^3$, and $He^3(n,d)D$ for each bombarding neutron energy.

For the gas filling used, the ranges[8] of the reaction products were plotted as a function of the laboratory angle, using the energy and angle as calculated from the kinematics of the process. For a given point in the counter where interactions may take place, one can determine that portion of the range of the reaction products which extends beyond the wall of the counter. This portion corresponds to the amount by which the detected pulse is reduced as compared with the pulse expected when all of the kinetic energy of the charged particles is expended in the counter. A spectrum was obtained for each point (or group of points with similar geometry) in the counter. The contributions from points outside the active volume of the counter, but within the gas volume, were also determined and found to be small. The spectra were weighted for (1) the solid angle, (2) the number of interactions within volumes of similar geometry, and (3) the probability that the particles of the reactions come off in a given solid angle.

The wall-effect spectrum was found to be relatively

[8] W. Whaling, *The Energy Loss of Charged Particles in Matter* (Kellogg Radiation Laboratory, California Institute of Technology, Pasadena, California).

TABLE IV. The ratios of cross sections to the total cross section.

E_n (Mev)	$\sigma_{(\text{elastic})}/\sigma_{(\text{total})}$	$\sigma[\text{He}^3(n,p)\text{H}^3]/\sigma_{(\text{total})}$	$\sigma[\text{He}^3(n,d)\text{D}]/\sigma_{(\text{total})}$
2.67	0.760±0.020	0.240±0.005	
5.00	0.835±0.017	0.144±0.011	0.0175±0.0063
8.07	0.848±0.012	0.114±0.012	0.038 ±0.003
17.50	0.8 ±0.1	$(\sigma_{n,p}+\sigma_{n,d})/\sigma_{(\text{total})}=0.2\pm0.1$	

insensitive to the assumed shape of the angular distribution for the $\text{He}^3(n,p)\text{H}^3$ reaction. Assuming an isotropic distribution as compared with a forward peaked distribution leads to only a 15% decrease in $d\sigma/d\Omega$ about $\theta_{\text{c.m.}}=110°$ for $E_n=8.0$ Mev, which is the region most sensitive to this correction. At other energies and angles, the difference is negligible. The total number of events interrupted by the walls is the same to within 1% for either assumed-angular distribution; thus the absolute cross section found for the $\text{He}^3(n,p)\text{H}^3$ reaction is not dependent upon this correction.

The final wall-effect spectrum obtained was then normalized by area to the full energy peak for the $\text{He}^3(n,p)\text{H}^3$ reaction that was experimentally observed in a region where no competing reaction occurs. The resulting wall-effect distributions for the $\text{He}^3(n,p)\text{H}^3$ reaction are shown in Figs. 7–10 by the dashed lines.

Corresponding calculations were also done for the $\text{He}^3(n,d)\text{D}$ and $\text{He}^3(n,n)\text{He}^3$ reactions. The resulting corrections in these cases were much smaller due to lower energies and shorter ranges of the reaction products.

D. Determination of Cross Sections vs Energy

For each energy, the total area under the curve of the number of $n+\text{He}^3$ reactions vs energy was measured after the subtraction of appropriate backgrounds. The ratio of the area of the He^3 recoil distribution to that of the total area then yields

$$\text{Recoil area/Total area}=\sigma_{\text{elastic}}/\sigma_{\text{total}}.$$

It is important to note that the uncertainty in the extrapolation to zero recoil energy introduces only a small uncertainty in the above ratio. Since the error made in this extrapolation is introduced in the same sense to both the recoil area and the total area, the ratio of these two quantities is therefore not greatly changed.

The ratios of the $\text{He}^3(n,p)\text{H}^3$ and $\text{He}^3(n,d)\text{D}$ cross sections to the total cross section were similarly obtained. These ratios and their uncertainties are listed in Table IV. The contribution of the $\text{He}^3(n,\gamma)\text{He}^4$ reaction as estimated from data on the inverse reaction is negligible.[9,10]

Absolute cross sections for each reaction were then obtained by normalizing to the known total cross section.[6] The total cross-section measurements were done by the transmission method, the quoted uncertainties being 2% at $E_n=2.6$ Mev increasing to 6% at 17.5 Mev. These uncertainties were included in the uncertainties listed for the various $n+\text{He}^3$ reaction cross sections determined in this experiment. All cross sections are listed in Table V and are plotted in Fig. 11.

Several collimators of the same length, but different materials and apertures were used in this experiment. (See Table III.) The final data were obtained using collimator A. The small aperture used sacrifices counting rate (a single spectrum was obtained in approximately 30 min with a 0.5-μa beam current) in order to keep the distortion of the spectra due to counter-wall effect to a minimum.

Data obtained when using larger apertures were corrected in the same manner as the final data, and the results were in excellent agreement. This gives justification for believing that the conclusions drawn from this experiment are not dependent upon the corrections made for the counter-wall effect.

TABLE V. Cross sections of $n+\text{He}^3$ reactions.

E_n (lab) (Mev)	Experimental cross sections (barns) Total (Ref. 6)	Elastic	$\text{He}^3(n,p)\text{H}^3$	$\text{He}^3(n,d)\text{D}$
0.95±0.02	2.85±0.06	2.24±0.14	0.61±0.08	···
2.67±0.02	3.06±0.06	2.33±0.10	0.73±0.03	···
5.00±0.02	2.36±0.06	1.97±0.09	0.34±0.04	0.041±0.016
8.07±0.02	1.86±0.06	1.58±0.06	0.21±0.03	0.071±0.008
17.50±0.05	0.98±0.06	0.8 ±0.1	0.2±0.1	

E_n (lab) (Mev)	Theoretical cross sections for elastic scattering (barns) (Ref. 2, 19) Type exchange: Serber	Sym-metrical	Cross sections from inverse reactions and other direct measurements (barns) $\text{He}^3(n,p)\text{H}^3$ (Ref. 5, 11)	$\text{He}^3(n,d)\text{D}$ (Ref. 12)
1.0	1.15	1.04	0.78±0.08	···
2.5	2.33	1.08	0.73±0.07	···
5.0	2.27	1.08	···	0.018±0.004
8.0	1.60	0.901	···	0.066 0.060±0.007
14.0	0.995	0.554	···	···
17.5	0.82	···	···	···

E. Differential Elastic-Scattering Cross Sections

The energy spectrum of the He^3 recoils is given by

$$E_R=E_n\frac{2mM}{(m+M)^2}(1-\cos\theta),$$

where the energies are in the laboratory system, θ is the center-of-mass scattering angle for neutrons, m and M the masses of the neutron and He^3 nuclei, respectively. The experimentally observed recoil distribution $N(E_R)$ in the laboratory system is proportional to $d\sigma/d\Omega$ in

[9] D. L. Livesley and I. G. Main, Bull. Am. Phys. Soc. **3**, 407 (1958); and Nuovo cimento **10**, 590 (1958).
[10] B. H. Flowers and F. Mandl, Proc. Roy. Soc. (London) **A206**, 131 (1951).

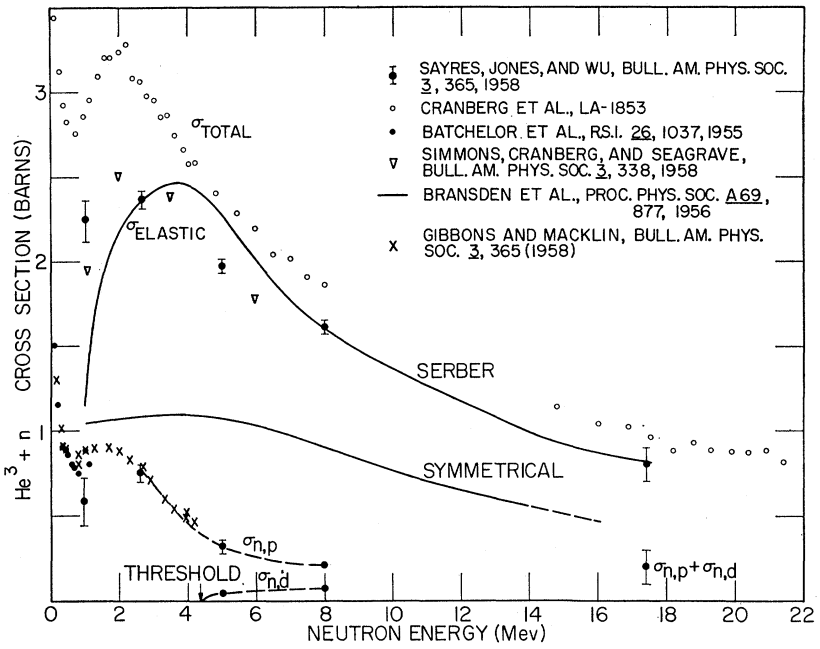

FIG. 11. The n+He^3 total, elastic, and reaction cross sections are plotted as a function of neutron energy. Also shown are the theoretical total elastic-scattering cross sections for both the Serber and symmetrical-type exchange forces as calculated by Bransden *et al.* (See references 2, 19.)

the center-of-mass system. Normalizing the shape of the recoil distribution to the previously obtained value for the elastic-scattering cross section thus gives $d\sigma/d\Omega$ as a function of $\cos\theta$ in the center-of-mass system. The experimentally obtained distributions were corrected for the distortion introduced by the finite resolution of the spectrometer. This correction was important only in the region of the maximum recoil energy. Corrections were also made for the distortion of the recoil distribution due to He^3 recoils striking the wall of the counter before expending all of their energy. Both of these corrections have very little effect upon the over-all shape of the angular distributions, being important only for $\theta \geq 150°$.

The wall-effect calculation for the n+He^3 reactions gives results which are in excellent agreement with the experimentally observed spectra, as can be seen in those regions where there is no ambiguity as to the origin of intensity; i.e., the $He^3(n,p)H^3$ wall-effect tail where no other reaction is present. For this reason, one can estimate that the calculated wall-effect distribution has an absolute uncertainty of about 10%; the uncertainty introduced into $d\sigma/d\Omega$ (elastic) being smaller than this. Table VI gives the percent error in the experimentally determined elastic differential cross sections brought about by the uncertainty in the pulse-height spectrum for the $He^3(n,p)H^3$ reaction when corrected for the counter-wall effect.

III. RESULTS

A. Reaction Cross Sections

Table V gives the results for the reaction cross sections and the corresponding values as calculated from the inverse reactions where such data are available. The cross-section data are also summarized in Fig. 11. The $He^3(n,p)H^3$ cross sections determined in this experiment are in good agreement with data from the inverse reaction[11] where such data are available. The value for the $He^3(n,d)D$ cross section at $E_n=5.0$ Mev is large compared with that calculated from the inverse reaction.[12] This disagreement is most probably due to the uncertainty in the subtraction of the recoil-distribution background, as may be seen in Fig. 8. Excellent agreement was obtained for the $He^3(n,d)D$ cross section at 8.0 Mev, where the recoil background subtraction is less uncertain. (See Fig. 9.)

B. Differential Cross Sections

The differential cross sections for the elastic scattering of neutrons by He^3 at laboratory energies E_n

TABLE VI. Uncertainties in $d\sigma/d\Omega$, for elastic scattering, due to the wall-effect corrections for the $He^3(n,p)H^3$ reaction.

$\theta_{c.m.}$ \ E_n (Mev)	2.6	5.0	8.0	17.5
60°	<1%	<1%	<3%	<6%
90°	<1%	···	5%	10%
100°	1%	2%	6%	···
110°	<1%	3%	6%	···
120°	<1%	3%	···	5%
150°	<1%	<3%	<3%	<5%

[11] J. H. Gibbons and R. L. Macklin (private communication), and Bull. Am. Phys. Soc. 3, 365 (1958).

[12] J. N. Bradbury and L. Stewart, Bull. Am. Phys. Soc. 3, 417 (1958); L. Stewart (private communication), and Los Alamos Scientific Laboratory LA-2014 (unpublished).

TABLE VII. Differential cross sections for the elastic scattering of neutrons by He^3 in the center-of-mass system (barns/steradian).

$\theta_{c.m.}$ (deg)	$E_n=2.6$ Mev $d\sigma/d\Omega$	$E_n=5.0$ Mev $d\sigma/d\Omega$	$E_n=8.0$ Mev $d\sigma/d\Omega$	$\theta_{c.m.}$ (deg)	$E_n=17.5$ Mev $d\sigma/d\Omega$
0[a]	0.418±0.025	0.455±0.060	0.407±0.060	12.9	0.201±0.030
5					
10					
15					
20					
25					
30					
35					
40			0.377±0.062		
48	0.318±0.020			45	0.134±0.018
50		0.360±0.080	0.254±0.010		
55	0.246±0.015	0.257±0.070	0.241±0.009	55	0.118±0.018
60	0.209±0.010	0.209±0.030	0.191±0.007	63	0.054±0.020
65	0.190±0.010	0.183±0.025	0.155±0.006		
70	0.168±0.010	0.145±0.025	0.110±0.005	70	0.040±0.020
75		0.115±0.015	0.087±0.007		
80		0.080±0.010	0.069±0.004	78	0.041±0.020
85			0.064±0.005	86	0.031±0.010
90	0.100±0.008		0.050±0.003		
95	0.085±0.004	0.045±0.005	0.041±0.003	93	0.012±0.004
100	0.085±0.004	0.040±0.004	0.035±0.003	100	0.009±0.003
105	0.098±0.004	0.042±0.004	0.025±0.003	107	0.009±0.002
110	0.101±0.004	0.038±0.004	0.026±0.003		
115	0.117±0.004	0.042±0.004		116	0.007±0.002
120	0.128±0.004	0.051±0.004		123	0.008±0.002
125	0.139±0.004	0.055±0.004			
130	0.159±0.005	0.060±0.004			
135	0.176±0.005	0.080±0.004	0.056±0.003	134	0.009±0.002
140	0.195±0.005	0.091±0.004	0.064±0.003		
145	0.209±0.005	0.105±0.005	0.072±0.003	143	0.010±0.002
150	0.230±0.010	0.120±0.008	0.083±0.005		
155		0.138±0.008	0.093±0.005		
160	0.257±0.010	0.148±0.010	0.103±0.006	159	0.018±0.002
165		0.162±0.010	0.111±0.006		
170		0.170±0.010			
175					
180	0.286±0.020	0.185±0.015	0.117±0.007	180	0.024±0.003

[a] Extrapolated from data.

=2.6, 5.0, 8.0, and 17.5 Mev are given in Table VII and plotted in Figs. 12, 13, 14, and 15, respectively, as a function of the center-of-mass angle in order to make possible a direct comparison of these results with the theoretical distributions as calculated by Bransden, Robertson, and Swan for $E_n=2.5$, 5.0, 8.0, and 14.0 Mev. The theoretical results are shown by the solid and dashed curves.

C. Linearity of the Pulse-Height Spectrum

The pulse heights of the peaks corresponding to the $He^3(n,p)H^3$ reaction and the $He^3(n,d)D$ reaction were proportional to the energy as calculated for each incident-neutron energy to within 0.5%. This was the accuracy to which a given pulse-height spectrum was reproduced on the 256-channel analyzer.

From the data, one finds that the pulse height for a He^3 recoil is also linear with energy on the same scale as for the other reactions. It is thus concluded that the mean energy to produce an ion pair in the counter gas for a He^3 nucleus is the same as that for a proton and triton. These results are in agreement with those of Jesse and Sadauskis,[13] who found that for noble gases the mean energy to form an ion pair for alpha particles and electrons is the same. These results are in disagreement with the conclusion suggested by Batchelor *et al.*[5] based on the data from their He^3-neutron spectrometer and the results of Tunnicliffe and Ward[14] for alpha particles and protons. Batchelor *et al.* chose, as the point corresponding to the maximum pulse height of the He^3 recoil distribution, the half-intensity point of the steeply descending slope of the end of the uncorrected recoil spectrum. It is this criterion of the maximum pulse height of the recoil distribution which brings about the disagreement.

In our case, by using various collimators of the same length, but different apertures, it was observed how the shape of the descending slope of the end of the recoil distribution is distorted by the counter-wall effect. Figure 16 shows the uncorrected recoil distributions obtained using the various collimators, as listed in Table III, for incident neutrons of energy 2.6 Mev.

[13] W. P. Jesse and J. Sadauskis, Phys. Rev. **97**, 1668 (1955).
[14] P. R. Tunnicliffe and A. G. Ward, Proc. Phys. Soc. (London) **A65**, 233 (1952).

From these spectra, it is seen that the bias at which the counting rate is halved shifts upward in pulse height as the aperture of the collimator is made smaller, i.e., as the distortion due to wall effect is reduced. The end point for the recoil distribution, when corrected for both the counter-wall effect and resolution, appears in the spectrum at the pulse height corresponding to the maximum energy of He^3 recoils ($E_R=\frac{3}{4}E_n$), where the pulse-height scale was determined from the pulse height of the fast-neutron peak for the $He^3(n,p)H^3$ reaction. These results show that the mean energy to form an ion pair in the gas filling is the same for protons, deuterons, tritons, and He^3 nuclei.

IV. DISCUSSION

The differential elastic-scattering cross sections fit the calculated distributions based on the Serber exchange force better than distributions calculated for the symmetrical exchange force, the agreement improving as the energy of the bombarding neutron is increased. However, the scattering at back angles falls somewhat below the theoretical distribution at all energies. Figure 11 shows the total elastic-scattering cross section as a function of energy. Here, the qualitative agreement with the total elastic-scattering cross section predicted from the Serber exchange force is best illustrated. The experimental results are in definite disagreement with the calculated total elastic-scattering cross sections expected for the symmetrical exchange force.

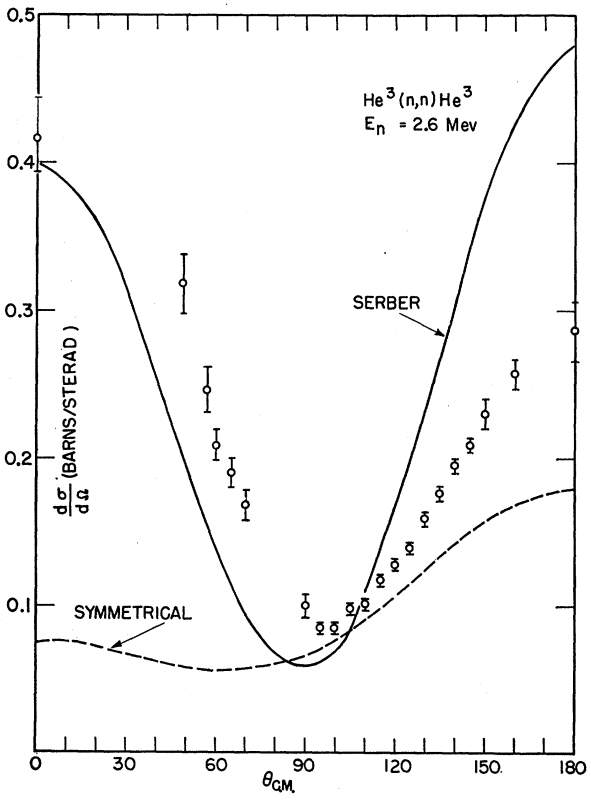

FIG. 12. The differential cross section for the elastic scattering of 2.67-Mev neutrons by He^3 is plotted as a function of the center-of-mass scattering angle. The point at $\theta=0°$ is extrapolated from the data. Also shown are the theoretical distributions of Bransden *et al.*

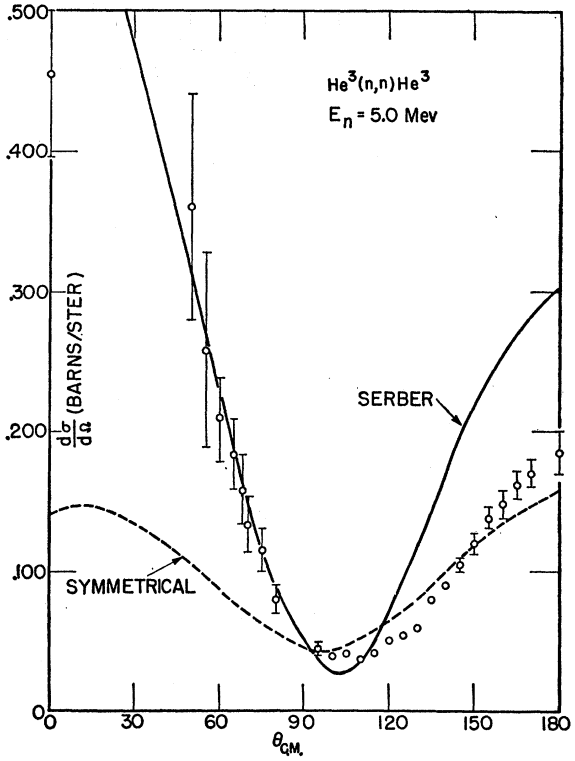

FIG. 13. The differential cross section for the elastic scattering of 5.0-Mev neutrons by He^3 is plotted as a function of the center-of-mass scattering angle. The point at $\theta=0°$ is extrapolated from the data. Also shown are the theoretical distributions.

Experimental results at $E_n=1.0$, 2.0, 3.5, and 6.0 Mev for elastic scattering of neutrons by He^3 and H^3 have been obtained at Los Alamos using the Los Alamos time-of-flight apparatus.[15] At 1 and 2 Mev, their results for the elastic scattering of neutrons are not in good agreement with the calculated distributions for either type exchange force. Their results at 3.5 and 6.0 Mev show the same qualitative shape of the distributions based on the Serber type exchange force as found here.[16] Closer agreement with the calculated distributions was obtained by the Los Alamos group for the scattering of neutrons by tritons, but again the scattering was smaller than predicted at back angles.

Bransden and Robertson[17] have made similar theo-

[15] J. E. Simmons, L. Cranberg, and J. D. Seagrave, Bull. Am. Phys. Soc. **3**, 338 (1958). J. D. Seagrave, J. E. Simmons, and L. Cranberg, Bull. Am. Phys. Soc. **3**, 338 (1958); Phys. Rev. **119**, 1981 (1960).

[16] A. Sayres, K. W. Jones, and C. S. Wu, Bull. Am. Phys. Soc. **3**, 365 (1958), (Report of Results).

[17] B. H. Bransden and H. H. Robertson, Proc. Phys. Soc. (London) **A72**, 770 (1958).

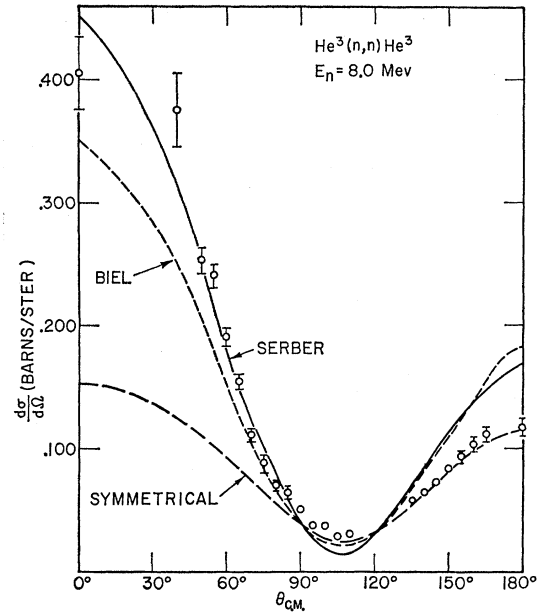

FIG. 14. The differential cross section for the elastic scattering of 8.07-Mev neutrons by He^3 is plotted as a function of the center-of-mass scattering angle. The point at $\theta=0°$ is extrapolated from the data. Also shown are the theoretical distributions.

retical calculations for elastic scattering of protons by tritons and He^3. A comparison with experimental data is made in their paper. More recent experimental results of Rosen *et al.*[18] for $p-T$ and $p-He^3$ scattering at $E_p=6.5$ and 8.3 Mev concur with the general conclusions drawn from the above theoretical calculations and previous experimental data.

In a more recent paper, Bransden, Hamilton, and Robertson[19] have presented similarly calculated angular

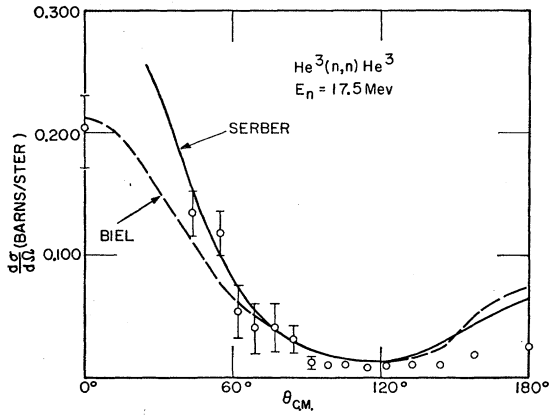

FIG. 15. The differential cross section for the elastic scattering of 17.50-Mev neutrons by He^3 is plotted as a function of the center-of-mass scattering angle. The point at $\theta=0°$ is extrapolated from the data. Also shown are the theoretical distributions of Bransden, Hamilton, and Robertson. (See reference 19.)

[18] L. Rosen (private communication), and L. Stewart, J. E. Brolley, and L. Rosen, Bull. Am. Phys. Soc. **4**, 104 (1959).
[19] B. H. Bransden, R. A. H. Hamilton, and H. H. Robertson, Proc. Phys. Soc. (London) **A75**, 144 (1960).

distributions for the scattering of nucleons by He^3 and H^3 at energies higher than previously reported.[2,17] Distributions based on the Serber exchange force were calculated for the scattering of neutrons by He^3 in order to compare with the 17.5-Mev data of this investigation,[16] and were calculated for $p-He^3$ and $p-H^3$ data at 19.4 Mev.[20] In addition, distributions based on a 70% Serber and 30% symmetrical exchange-force mixture were also calculated. This mixture was found by Biel[21] to give the correct binding energies of Be^8 and C^{12}.

The distributions based on the Serber exchange force at 17.5 Mev and the Biel exchange force at 8.0 and 17.5 Mev are shown in Figs. 14 and 15 along with the previously discussed experimental data. The calculated $n-He^3$ total elastic-scattering cross section of 0.82 b

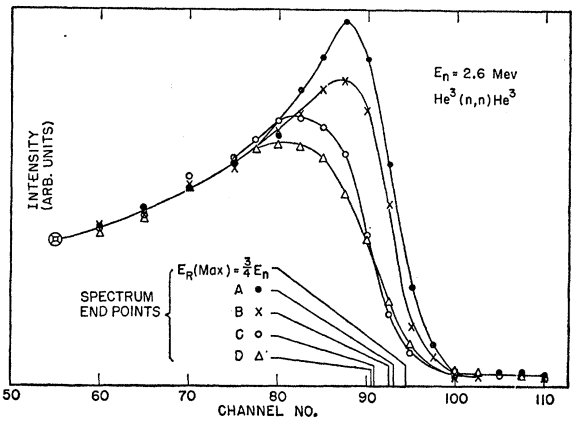

FIG. 16. Uncorrected He^3-recoil distributions obtained using various collimators as listed in Table III. The curves were normalized to unit intensity at channel 55 and plotted on an expanded scale. The end point of each spectrum as determined by the point of half-intensity is shown for each collimator used, as is the point $(\frac{3}{4}E_n)$ determined by the position of the peak for the $He^3(n,p)H^3$ reaction for $E_n=2.67$ Mev.

at $E_n=17.5$ Mev for the Serber exchange force is in excellent agreement with the experimental value of 0.8 ± 0.1 b found here. The comparison of the calculated distributions at these higher energies with the experimental data shows better agreement with the distributions based on the Serber exchange force than with the Biel exchange mixture.

In conclusion, the $n-He^3$ and $p-T$ scattering is not as well described by the calculations at lower energies as is the $p-He^3$ and $n-T$ scattering. From the results of this experiment on the interaction of neutrons with He^3, one can see that as the cross section for the $He^3(n,p)H^3$ reaction becomes a smaller fraction of the total cross section, with increasing neutron energy, the experimental data for the elastic scattering of neutrons

[20] R. A. Vanetsian and E. D. Fedchenko, Soviet J. Atomic Energy (English Translation) **2**, 141 (1957).
[21] S. J. Biel, Proc. Phys. Soc. (London) **A70**, 866 (1957).

by He^3 more closely follow the theoretical curves obtained, based on the Serber interaction.

These experimental results suggest that the influence of the charge exchange reaction, $n+He^3 \leftrightarrow p+T$, is indeed important. Inclusion of this and the $n+He^3 \leftrightarrow D+D$ reaction in the theory may bring the $n-He^3$ and $p-T$ results to as close agreement with the theoretical distributions based on the Serber exchange force as is found for the $p-He^3$ and $n-T$ results. A study of the effect of the charge exchange reaction and the $He^3(n,d)D$ reaction on the theoretical distributions expected for elastic scattering is reported to be in progress.[22]

[22] B. H. Bransden (private communication).

PHYSICAL REVIEW VOLUME 122, NUMBER 6 JUNE 15, 1961

Decay of I^{132}

R. L. Robinson, E. Eichler, and Noah R. Johnson
Oak Ridge National Laboratory, Oak Ridge, Tennessee

(Received January 18, 1961; revised manuscript received March 17, 1961)

The decay of I^{132} has been investigated by means of scintillation spectrometers. Energies (and relative intensities) of the gamma rays which were observed are 0.240(1.3), 0.518(15), 0.667(100), 0.72(5), 0.775(63), 0.953(15), 1.14(1.2), 1.142(2.7), 1.30(2.4), 1.392(6.4), 1.45(1.1), 1.75(0.3), 1.91(0.7), 1.99(0.8), 2.08(0.18), 2.18(0.13), and 2.39(0.11) Mev. Our data indicate that the gamma-ray peak at 0.667 Mev actually consists of four gamma rays with energies between 0.62 and 0.68 Mev. An energy level diagram of Xe^{132} based on the present spectral studies and gamma-gamma angular correlation measurements has been proposed. Energies (and spins) of the levels are 0.673(2+), 1.32, 1.448(4+), 1.81, 1.966(3), 2.10(3 or 4), 2.401(4), 2.59(3), and 2.84(3, 4, or 5) Mev.

I. INTRODUCTION

During the past few years several nuclear models have been developed to explain the experimentally observed properties of low-lying levels in even-even, medium-weight nuclei. To determine the range of applicability of these different models and to provide information which can be used to guide future development of nuclear models, additional experimental studies of these nuclei are needed. In the present work, levels of the even-even nucleus Xe^{132} which are populated by the decay of 2.3-hr I^{132} have been studied by means of scintillation spectrometers. An energy-level diagram which incorporates the results of this study has been proposed.[1]

The most extensive previous investigation of the decay of I^{132} was made by Finston and Bernstein.[2] Their decay scheme is illustrated in Fig. 1. The first excited state of Xe^{132} has also been observed in Coulomb excitation studies.[3] A value of four has been measured for the ground-state spin of I^{132} by Sherwood, Ovenshine, and Parker,[4] and by Lipworth, Garvin, and Nierenberg.[5]

[1] A brief account of some of these measurements was presented at the 1960 Conference of the Southeastern Section of the American Physical Society [R. L. Robinson, E. Eichler, and N. R. Johnson, Bull. Am. Phys. Soc. **5**, 448 (1960)].
[2] H. L. Finston and W. Bernstein, Phys. Rev. **96**, 71 (1954).
[3] G. F. Pieper, C. E. Anderson, and N. P. Heydenburg, Bull. Am. Phys. Soc. **3**, 38 (1958).
[4] J. E. Sherwood, S. J. Ovenshine, and G. W. Parker, Bull. Am. Phys. Soc. **4**, 386 (1959).
[5] E. Lipworth, H. L. Garvin, and W. A. Nierenberg, Bull. Am. Phys. Soc. **4**, 353 (1959).

II. EXPERIMENTAL PROCEDURE AND RESULTS

A. Source Preparation

Fission-product Te^{132} was obtained from Brookhaven National Laboratory. Tellurium and iodine carrier was added to an aliquot and the solution made strongly basic. Sodium hypochlorite was added to oxidize the tellurium and iodine to insure good exchange of activity and carrier. The solution was then acidified and Te metal precipitated by treatment with SO_2 gas. After the precipitate was washed, it was dissolved in a small amount of concentrated HNO_3. Iodine carrier was added and extracted into CCl_4. This CCl_4 solution contained the long-lived iodine isotopes—I^{131} and I^{133}—that had grown in during processing and shipment of the source material.

After an adequate growth period, more iodine carrier was added and a CCl_4 extraction performed. Next the CCl_4 phase was removed and washed with water, and the I^{132} activity was back-extracted into the aqueous phase by addition of sodium metabisulfite. Finally, $AgNO_3$ solution was added to precipitate AgI. Sources of AgI mounted on 6.5 mg/cm^2 Mylar tape were used for singles spectra and most gamma-gamma coincidence spectra. Sources of tellurium metal containing Te^{132}–I^{132} equilibrium mixture mounted on Mylar tape were used for beta-gamma and gamma-gamma-gamma coincidence spectra.

B. Gamma-Ray Spectra

The gamma rays were detected with 3 in.$\times$3 in. NaI crystals which were mounted on 6363 DuMont photo-